

**Multi-hole probes
with RPA**

N. Wildmann et al.

This discussion paper is/has been under review for the journal Atmospheric Measurement Techniques (AMT). Please refer to the corresponding final paper in AMT if available.

Towards higher accuracy and better frequency response with standard multi-hole probes in turbulence measurement with Remotely Piloted Aircraft (RPA)

N. Wildmann, S. Ravi, and J. Bange

Center for Applied Geoscience, Eberhard-Karls-Universität Tübingen, Germany

Received: 8 August 2013 – Accepted: 5 November 2013 – Published: 14 November 2013

Correspondence to: N. Wildmann (norman.wildmann@uni-tuebingen.de)

Published by Copernicus Publications on behalf of the European Geosciences Union.

Title Page

Abstract

Introduction

Conclusions

References

Tables

Figures

◀

▶

◀

▶

Back

Close

Full Screen / Esc

Printer-friendly Version

Interactive Discussion



Abstract

This study deals with the problem of turbulence measurement with small remotely piloted aircraft (RPA). It shows how multi-hole probes (MHPs) can be used to measure fluctuating parts of the airflow in flight up to 20 Hz. Accurate measurement of the transient wind in the outdoor environment is needed for the estimation of the 3-D wind vector as well as fluxes of heat, momentum, water vapour, etc. In comparison to an established MHP system, experiments were done to show how developments of the system setup can improve data quality. The study includes a re-evaluation of the pneumatic tubing setup, the conversion from pressures to airspeed, the pressure transducers, and the data acquisition system. In each of these fields, the steps that were taken lead to significant improvements. A spectral analysis of airspeed data obtained in flight tests shows the capability of the system to measure atmospheric turbulence up to the desired frequency range.

1 Introduction

In many applications multi-hole probes (MHPs) serve the purpose of measuring the flow angle and speed of an airstream. They are commonly used in windtunnel and road tests for the automotive industry (Zimmer et al., 2001) as well as in airborne measurements (Crawford and Dobosy, 1992). Many different designs and calibration techniques can be found in literature (Telionis et al., 2009; Sumner, 2000; Pfau et al., 2002; Lemonis et al., 2002). The minimum number of holes that are used for three dimensional flow measurement is four, while probes with five holes are common and seven hole probes can also be found. With increasing number of holes, the range of the angle of incidence that can still be measured with the probe increases. There are also probes with only one pressure port, which is constantly turned inside the probe (Schlienger et al., 2002). The shape of the probe (conical, hemispherical or faceted) has an effect on the maximum incidence angle as well as on the sensitivity

AMTD

6, 9783–9818, 2013

Multi-hole probes with RPA

N. Wildmann et al.

Title Page

Abstract

Introduction

Conclusions

References

Tables

Figures

◀

▶

◀

▶

Back

Close

Full Screen / Esc

Printer-friendly Version

Interactive Discussion



Multi-hole probes
with RPA

N. Wildmann et al.

Title Page

Abstract

Introduction

Conclusions

References

Tables

Figures

◀

▶

◀

▶

Back

Close

Full Screen / Esc

Printer-friendly Version

Interactive Discussion



surface and is determined using the on-board navigation system. Aboard an RPA the latter is usually a combination of an inertial measurement unit (IMU) and a global navigation satellite system (GNSS). The determination of the ground speed \mathbf{v}_{gs} and the rotation into the earth's coordinate system \mathbf{M}_{mf} using the Eulerian angles are not subject of the present study, and are described in literature (Haering, 1990; Leise and Masters, 1993; Boiffier, 1998; van den Kroonenberg et al., 2008; Bange, 2009).

The true-airspeed vector \mathbf{v}_{tas} is the flow vector measured by an in situ flow probe, in this study a MHP, preferably mounted at the nose of the RPA. Thus \mathbf{v}_{tas} is defined in the aircraft's coordinate system f . The location of the MHP in relation to the origin of the aircraft-fixed coordinate system f is described by the lever-arm vector $\mathbf{s}_p = (x_p, y_p, z_p)$ which points from the origin of the aircraft system f to the location of the MHP. The vector of angular rotation rates $\mathbf{\Omega}$ contains the angular velocities of the aircraft system f related to the meteorological system m and is among the primary output data of the IMU.

In the following we focus on the determination of the true-airspeed vector \mathbf{v}_{tas} defined by

$$\mathbf{v}_{tas} = - \frac{|\mathbf{v}_{tas}|}{\sqrt{1 + \tan^2 \alpha + \tan^2 \beta}} \begin{pmatrix} 1 \\ \tan \beta \\ \tan \alpha \end{pmatrix} \quad (2)$$

(see also Lenschow, 1986; Leise and Masters, 1993; Williams and Marcotte, 2000; van den Kroonenberg et al., 2008; Bange, 2009), with angle of attack α (positive for air flow from below) and sideslip β (positive for flow from starboard). All three variables $\alpha, \beta, |\mathbf{v}_{tas}|$ in Eq. (2) can be derived from MHP pressure measurements.

Research RPA MASC

At the University of Tübingen the research platform MASC (Multi-purpose Airborne Sensor Carrier) is operated and equipped with a MHP, fast temperature sensors,

2.2 Differential pressure to flow angle conversion

The conversion between differential pressures of the six pressure ports of the probe to flow angles and true airspeed is usually based on wind tunnel calibration and can be done in several ways (see Sasangko, 1997; Bohn and Simon, 1975; Treaster and Yocum, 1979). A typical solution is a polynomial fit between normalized pressure differences and airflow angles, true airspeed and static pressure respectively. The ISM probe was intensively used in field campaigns (e.g. Martin et al., 2011; van den Kroonenberg et al., 2011; Spieß et al., 2007) with the M^2AV . Table 1 shows how dimensionless coefficients are defined from the pressures at the probe. The definitions on the left are taken from Bohn and Simon (1975), for an English summary, see Spieß (2006). They are referred to as the M^2AV conversion method in the following. The definition of the pressure ports and differential pressures is described in Figs. 4 and 5. The coefficients k_α and k_β are directly calculated from the pressures at the MHP ports (see Table 1 for different methods to do so). Using a polynomial fit with coefficients that were determined in a windtunnel calibration, the angle of sideslip, angle of attack and the coefficients k_q and k_p can be calculated from k_α and k_β .

$$\begin{aligned}\alpha &= f_\alpha(k_\alpha, k_\beta) \\ \beta &= f_\beta(k_\alpha, k_\beta) \\ k_p &= f_s(k_\alpha, k_\beta) \\ k_q &= f_q(k_\alpha, k_\beta)\end{aligned}\quad (3)$$

To find dynamic and static pressure, the expressions for k_q and k_p in Table 1 need to be solved for q and p respectively. The true airspeed as used in Eq. (2) has to be calculated using the measured total air temperature T_{tot} , the static pressure p and the

Title Page

Abstract

Introduction

Conclusions

References

Tables

Figures

◀

▶

◀

▶

Back

Close

Full Screen / Esc

Printer-friendly Version

Interactive Discussion



dynamic pressure q :

$$|\mathbf{v}_{\text{tas}}|^2 = 2c_p T_{\text{tot}} \left[1 - \left(\frac{p}{p+q} \right)^\kappa \right] \quad (4)$$

with the Poisson number $\kappa = R/c_p$, where $R = 287 \text{ J kg}^{-1} \text{ K}^{-1}$ is the gas constant for dry air and $c_p = 1005 \text{ J kg}^{-1} \text{ K}^{-1}$ is the specific heat for dry air.

In the M^2AV conversion the ring pressure ports are used to find q and p to get a more angle-independent measurement. However, it was identified that in certain flight conditions the ring can cause problems for turbulence measurement, since the ring port pressure shows an increased noise level, which is induced by the probe itself. Figure 6 shows the result of measurements during the calibration procedure of the MHP in a jet windtunnel with a turbulence intensity of about 1%. At a constant airspeed of 22 m s^{-1} and angle of attack of 10° the angle of sideslip β was varied between -20° and 20° in steps of 2° . Each position was held for ten seconds and the standard deviation of the ring port pressure was measured. It can be seen that at certain angles of sideslip, the fluctuations of the measured pressure is higher than at other angles. This can be considered to be aerodynamic noise introduced by the probe.

To avoid measuring turbulence that is not primarily atmosphere related, a different pressure conversion method (see Table 1, right column) that avoids using the ring port pressure was tested. The method was initially proposed by Treaster and Yocum (1979) and is one of the most basic five hole probe calibration methods. It only uses one front hole and four side holes.

Figure ?? shows the measurement of the airflow angles and true airspeed in one flight leg of 1000 m (including parts of the turns at the beginning and the end). The flight was done at late afternoon on 23 September close to the observatory Lindenberg of the German Meteorological Service. The flight altitude was 100 m above ground in an atmospheric boundary layer with weak stability.

The pressures from the five hole probe were converted in both ways, with the M^2AV method and with the MASC method, avoiding ring port measurements. While the

Multi-hole probes with RPA

N. Wildmann et al.

Title Page

Abstract

Introduction

Conclusions

References

Tables

Figures

◀

▶

◀

▶

Back

Close

Full Screen / Esc

Printer-friendly Version

Interactive Discussion



Multi-hole probes
with RPA

N. Wildmann et al.

Title Page

Abstract

Introduction

Conclusions

References

Tables

Figures

◀

▶

◀

▶

Back

Close

Full Screen / Esc

Printer-friendly Version

Interactive Discussion



airflow angles do not show a difference, it can clearly be seen that true airspeed is much less noisy in the latter method. The spectra of the velocities estimated through the M^2AV (Fig. 9) shows that the noise introduced by the ring pressure ports manifest as “white-noise” at higher frequencies, while the MASC method shows significantly

5 reduced noise and the presence of the $k^{-\frac{5}{3}}$ slope (Kolmogorov distribution for locally isotropic turbulence in the inertial subrange).

It should be noted that the large difference between the two methods shows up explicitly at certain airflow angles, which were included in the presented time series. However, even though errors are smaller at other angle combinations, they can be

10 completely avoided if the ring port pressure is not used for true airspeed calculation.

3 Tubing response and calibration of the probe

As transient velocities are of particular interest, the pneumatic dynamic response of tubing and transducer needs to be investigated to ensure measurements within a certain error band in the target frequency range. The tubing system within the MHP consists of a combination of a steel tube of inner diameter 0.7 mm and another tube of different material (e.g. PVC) and diameter. The dynamic response of the system depends on not only the length and diameter of the tubing, but also on the air volume inside the pressure transducers. The magnitude and phase response of tubing systems has been well investigated by Bergh and Tijdeman (1965). They derived theoretical estimates of

15 the response of a single tube connected to either a single or multiple transducers connected in series with the variable tubing length, tubing diameter and transducer volume. Further studies investigated the validity of the model for short tubing length and proved it suitable for tubing longer than 150 mm (Semaan and Scholz, 2012). However, their model does not account for branched tubing systems.

25 Since differential pressures are required for airflow angle estimation, one strategy would be to connect the holes of a five hole probe to pressure transducers and calculate the flow angles from the measured differential pressures as described in Spieß et al.

by piezoresistivity. The LBA sensors estimate pressure difference through a thermal mass flow measurement.

To visualize the response of the pressure measurement system, the amplitude and phase response as the two parts of the transfer function H of the system are calculated:

$$5 \quad H(\omega) = |H(\omega)|e^{i\phi(\omega)} \quad (6)$$

where ω is the angular frequency and ϕ the phase shift. The amplitude response is presented as the ratio between the standard deviation σ of the tubing system being investigated and the reference:

$$10 \quad |H(\omega)| = \frac{\sigma_{P0}(\omega)}{\sigma_{P_{ref}}(\omega)} \quad (7)$$

To find the phase response of the system, the cross-correlation function $Q_{P0,P_{ref}}$ between the two sensors was calculated for each frequency and the time shift between the two signals needed for maximum correlation was estimated. This time shift was converted to a phase angle in the following manner:

$$15 \quad \Delta t = t(\max|Q_{P0,P_{ref}}|) \quad (8)$$

$$\phi = \Delta t \cdot \omega \cdot \frac{180}{\pi} \quad (9)$$

The tests with the P4V-Mini sensors showed considerable variations in the response of each individual transducer. Therefore, the experiment was carried out with the LBA sensors by Sorsortechtechnics only. Section 4 will give more reasons why in flight measurements this type of sensors is chosen in future. The amplitude and phase response of the two tubing systems are presented in Fig. 11. In the same figure, the theoretical response for the single tube of same length without branches as calculated with the Bergh and Tijdenman model is presented.

25 It can be seen that both tubing setups resemble oscillatory dynamic systems with at least one resonance frequency. The first resonant frequency of the M²AV system was

Multi-hole probes with RPA

N. Wildmann et al.

Title Page

Abstract

Introduction

Conclusions

References

Tables

Figures

◀

▶

◀

▶

Back

Close

Full Screen / Esc

Printer-friendly Version

Interactive Discussion



found to be at around 80 Hz, while it is out of the measurement range for the alternative setup. The damping factor of the M^2AV setup is much higher than for the alternative setup, hence the resonance amplitude was much smaller. The phase response attenuates towards -180° , which is characteristic for a second order dynamical system.

It should be recalled that in the M^2AV setup, one side of the differential transducers was connected to the side holes of the probe directly, while the other side of the transducers was connected to the front hole with a branch to five other transducers. In light of the acoustic tests performed here, it was identified that the tubing responses on either side of the transducer differ significantly. Though the two tubing systems have nominally similar amplitude response, a phase shift φ between each other would exist. Therefore an artificial signal S_m would be measured, that can be described as follows:

$$\begin{aligned} S_m &= \sin \omega t - \sin(\omega t + \varphi) \\ &= \sin \omega t - \sin \omega t \cdot \cos \varphi + \cos \omega t \sin \varphi \\ &= (1 - \cos \varphi) \sin \omega t + \sin \varphi \cos \omega t \end{aligned}$$

knowing that:

$$a \cdot \sin \omega t + b \cdot \cos \omega t = A \cos(\omega t - \alpha)$$

with:

$$A = \sqrt{a^2 + b^2} \quad (10)$$

$$\tan \alpha = \frac{b}{a} \quad (11)$$

the artificial signal is:

$$\begin{aligned} S_m &= \sqrt{(1 - \cos \varphi)^2 + \sin^2 \varphi} \cdot \cos \left[\omega t - \arctan \frac{\sin \varphi}{1 - \cos \varphi} \right] \\ &= \sqrt{2(1 - \cos \varphi)} \cdot \cos \left[\omega t - \cot^{-1} \frac{\varphi}{2} \right] = 2 \sin \frac{\varphi}{2} \cdot \cos \left[\omega t - \cot^{-1} \frac{\varphi}{2} \right] \end{aligned} \quad (12)$$

Multi-hole probes with RPA

N. Wildmann et al.

Title Page

Abstract

Introduction

Conclusions

References

Tables

Figures

◀

▶

◀

▶

Back

Close

Full Screen / Esc

Printer-friendly Version

Interactive Discussion



Multi-hole probes
with RPA

N. Wildmann et al.

Title Page

Abstract

Introduction

Conclusions

References

Tables

Figures

◀

▶

◀

▶

Back

Close

Full Screen / Esc

Printer-friendly Version

Interactive Discussion



From Fig. 11, at 20 Hz the two tubing connections have a difference in phase shift of about 10° . This implies, the transducer would measure a differential signal with an amplitude of $2 \sin \frac{10^\circ}{2} = 0.174$ times the original absolute signal, which is added to the measurement and can thereby be defined as an error of almost 20 %.

To see the real behaviour of the two tubing strategies and the artificial signals that are measured due to phase shift effects, a setup equal to that present in the M^2AV was tested. That is, both ends of a transducer were connected to the acoustic box whereby one port was connected to the box through a branch with five other transducers connected in parallel and the other port of the transducer was directly connected to the acoustic box via a 18 cm tube. In subsequent tests, both ports of the transducers were connected via 18 cm tubes to the acoustic box, this would resemble the alternate tubing strategy that is now being used on MASC. Ideally, as both ends of the transducers are connected to the same “source” (acoustic box), the pressures in the transducers should nullify one another and no pressures should be logged. The results of a time series measuring a sweep from 10 to 100 Hz (in steps of 10 Hz and a rest time of 10 s at each step) are shown in Fig. 12, left. The increase in amplitude of the pressure signal is not only due to an increasing phase shift, but also due to the increasing power of the speaker at the same gain setting. Figure 12, right, shows a normalized result for the measured frequency range, where the measured signal was divided by the prevailing pressure in the box that was measured with a second transducer. It can be seen that the relative error for 20 Hz is less than theoretically estimated, but it is also obvious that the effect can be observed in real measurements and can be avoided with the point to point tubing connections.

4 The pressure transducers

The volume of the pressure transducers adds to the pneumatic transfer function, and variation between different transducers can lead to significantly different amplitude and phase response of the sensor at higher frequencies. Besides that, most pressure

**Multi-hole probes
with RPA**

N. Wildmann et al.

Title Page

Abstract

Introduction

Conclusions

References

Tables

Figures

◀

▶

◀

▶

Back

Close

Full Screen / Esc

Printer-friendly Version

Interactive Discussion



transducers are also sensitive to vibrations. In many MEMS-based differential pressure transducers, deformation of a membrane exposed to the applied pressure is measured by the means of piezoelectricity (in our study the sensor of type P4V-Mini, as used in the M²AV for example). The piezoelectric voltage is amplified and a voltage linear to the applied pressure is put out by the sensor. However, the membrane can also be deformed by accelerations perpendicular to the membrane surface. Since aircraft are always subject to vibrations and accelerations it is important to consider this effect in the pressure measurements when membrane based pressure transducers are used. The way to reduce the errors made due to this effect can be to calibrate the sensors for the sensitivity regarding acceleration and measure the given accelerations in flight to subtract the acceleration induced signal from the transducer output signal. A way to avoid the issue of sensitivity to accelerations completely is to choose a different measuring principle which is not based on a membrane deformation. A suitable alternative are sensors that work on thermal flow measurement (in our study the sensor of type LBA, as used in MASC). Figure 13 shows a comparison between a membrane based sensor and a thermal flow sensor which were at the same time exposed to accelerations by mounting them at one solid board and knocking it on the table in three different orientations. It can be seen that the accelerations in the orientation perpendicular to the membrane orientation (here the y-direction) affect the membrane based sensor, but not the thermal flow sensor. In the test, accelerations up to 5 ms⁻² were applied. Similar accelerations can be found in straight leg flights with the system MASC. Other aircraft might have less or more vibration depending on the propulsion and flight dynamics. The resulting pressure transducer noise with amplitudes up to 3 Pa adds to the higher frequency turbulence measurement and will cause higher relative errors at lower turbulence intensity.

5 Sampling and anti-aliasing

So far, errors by aerodynamic and mechanical effects were discussed that affect the signal that is passed on by the pressure transducer. The next step in the measuring chain is to convert this analog 0–5 V signal from the pressure transducer to a digital signal and logging the data of all channels synchronously to one file. All data acquiring systems (DAQ) need to address the effect of aliasing in the measured frequency scales. Aliasing is critical in two ways: first, high frequency noise signals can alias into the sampled frequency range, if they are not filtered. Second, the signal of the physical variable to be measured with frequencies slightly higher than half the sampling frequency can fold into the sampled frequency range and then lead to overestimates in the power of the signal at low frequencies. Commercial DAQ are generally unsuitable for RPA because they are either too heavy, too big or need too much power. The University of Tübingen developed the measuring computer AMOC (Airborne Meteorological Onboard Computer) in cooperation with the University of Applied Sciences Ostwestfalen-Lippe. The computer is equipped with two STM32 microcontrollers, a 24 bit, 16 channel analog to digital converter, a telemetry interface, an SD-card slot for data logging and various other interfaces (see also Wildmann et al., 2013). To obtain reliable turbulence measurements within an error band of 10 %, an anti-aliasing filter was designed and implemented on the measuring computer which contains the following parts:

1. A first order analog filter (RC-low pass) with cut-off frequency at 160 Hz:
Only 50 % of the original amplitude of signals with 160 Hz passes the filter, only 10 % of the signal at 500 Hz. The amplitude response of the analog filter can be seen in Fig. 14 as a dashed blue line.
2. Oversampling of the signal at 500 Hz onboard the measuring computer:
Only signals above 500 Hz appear as aliases in the measured signal onboard the measuring computer. As described above, these signals are already damped to less than 10 % of the original signal.

Title Page

Abstract

Introduction

Conclusions

References

Tables

Figures

◀

▶

◀

▶

Back

Close

Full Screen / Esc

Printer-friendly Version

Interactive Discussion



Multi-hole probes
with RPA

N. Wildmann et al.

Title Page

Abstract

Introduction

Conclusions

References

Tables

Figures

◀

▶

◀

▶

Back

Close

Full Screen / Esc

Printer-friendly Version

Interactive Discussion



3. Digital moving average filter with cut-off frequency at 70 Hz in real-time onboard AMOC:

The moving average filter is chosen because of its simple implementation, needing only little computing power in real-time processing and giving an optimal noise reduction while keeping sharp step responses (Smith, 1997). The rather poor performance of the filter in frequency separation is still good enough for the given task. From the red dashed line in Fig. 14, it can be seen that the filter still has a quasi flat response at 10 Hz and still more than 91 % of the signal amplitude is passed at 20 Hz, while at 100 Hz only 25 % pass and thanks to the complementary analog filter, the response of signals above 150 Hz is always damped to a maximum of 6 % of the original signal.

4. The log onto the SD-card at 100 Hz:

Logging at 100 Hz is another oversampling step to achieve anti-aliased data up to 20 Hz at least. Sampling at 100 Hz, signals between 100 Hz and 150 Hz can fold into the frequency range above 50 Hz only. The previous steps explained how signals above 150 Hz are already damped to less than 6 % and therefore have very little impact.

This means that in the frequency range from 0 Hz to 50 Hz, a maximum error caused by aliasing of 6 % is theoretically possible. In reality, the measured signal is a turbulent flow, wherein the power of the signal decreases with increasing frequency frequency (power law $k^{-5/3}$ in the inertial sub-range of locally isotropic turbulence, Kolmogorov, 1941).. This means that the aliases naturally have a lower amplitude compared to the true signal at a specific frequency, which also means that the maximum error that was estimated is overestimated, except for unnatural noise signals. Note that electromagnetic noise typically begins at much higher frequencies that are filtered by the analog filter.

6 Comparison of MASC and M²AV data

In order to demonstrate that the design considerations in the airflow measurement system, as described above, do show the desired improvement in turbulence measurement, an analysis of the frequency response of the system in flight was carried out. Kolmogorov's theory of locally isotropic turbulence in the inertial subrange provides theoretical slopes of variance spectrum and structure function. If measured data is compared to this theory, the quality of turbulence measurement can be evaluated. Figure 15 shows the result of this analysis for true airspeed measurement. To prove that real enhancements compared to established measurement systems like the M²AV were achieved, the result is compared to measurements of the M²AV in very similar meteorological conditions. The M²AV flight was in summer on 10 July 2010. The MASC flight in late spring, 8 May 2013, both in the already mixed layer in the late morning at an altitude of 200 m and 100 m respectively. It can be seen that the MASC system follows theory very well up to 10 Hz. Slight damping according to the theory in Sect. 5 can be observed at higher frequencies. According to the experiments that were done, comparing tubing strategy, pressure transducers and probe calibration, it would be expected that the M²AV system is subject to more noise. The data does not reflect this. Instead, in the structure function, a strong damping is observed in the system at 2–3 Hz. This suggests that the noise was reduced by a low pass filter in the pressure measurements of the probe. This cannot be ascertained in the absence of more information on the DAQ used in the M2AV. However, it can be stated that the MASC MHP setup meets the desired frequency response better than the M²AV system.

7 Conclusions

It was shown in this study how a standard MHP can be optimized for turbulence measurements with a few easy actions. It is of high importance to know the frequency response of each piece in the measuring chain, starting with the pneumatic response of

AMTD

6, 9783–9818, 2013

Multi-hole probes with RPA

N. Wildmann et al.

Title Page

Abstract

Introduction

Conclusions

References

Tables

Figures

◀

▶

◀

▶

Back

Close

Full Screen / Esc

Printer-friendly Version

Interactive Discussion



Multi-hole probes
with RPA

N. Wildmann et al.

Title Page

Abstract

Introduction

Conclusions

References

Tables

Figures

◀

▶

◀

▶

Back

Close

Full Screen / Esc

Printer-friendly Version

Interactive Discussion



the MHP itself, the tubing and the pressure transducers. The common error of vibration sensitivity in membrane based pressure transducers was discussed, and we suggest to use thermal flow sensors instead to avoid this effect. It was also shown how the data acquisition has to be optimized for non-disturbed turbulence measurement in the desired frequency range. The effect of anti-aliasing can be minimized by an appropriate filter design. Considering these points, precise measurements of mean flow and turbulent fluctuation up to 20 Hz can be achieved with the given MHP and DAQ system. To use the MHP in RPA applications for wind and flux measurement, it has to be embedded into a measurement system consisting of the aircraft itself, inertial measurements and an autopilot in best case. Questions like flow distortion by the fuselage and wings has to be discussed for each individual aircraft type. The fusion of airflow data with inertial measurements to calculate wind is already described by van den Kroonenberg et al. (2008).

Acknowledgements. We would like to thank Maximilian Ehrle and Markus Auer for their great job as safety pilot and Bernd Peters and the IAG Stuttgart for the support and time with the jet windtunnel. The measuring equipment would not have been ready to work without the help of Jens Dünnermann and Burkhard Wrenger from the University of Applied Sciences Ostwestfalen-Lippe. We acknowledge the support from Peter Scholz at the University of Braunschweig for questions regarding the MHP design.

We acknowledge support by Deutsche Forschungsgemeinschaft and Open Access Publishing Fund of Tuebingen University.

References

- Bange, J.: Airborne Measurement of Turbulent Energy Exchange between the Earth Surface and the Atmosphere, Sierke Verlag, 174 pp., ISBN 978-3-86844-221-2, Göttingen, Germany, 2009. 9786
- Bergh, H. and Tijdeman, H.: Theoretical and Experimental Results for the Dynamic Response of Pressure Measuring Systems, Vol. 238, National Lucht- en Ruimtevaartlaboratorium, Amsterdam, Netherlands, 1965. 9790

Multi-hole probes with RPA

N. Wildmann et al.

Title Page

Abstract

Introduction

Conclusions

References

Tables

Figures

◀

▶

◀

▶

Back

Close

Full Screen / Esc

Printer-friendly Version

Interactive Discussion



Bohn, D. and Simon, H.: Mehrparametrische Approximation der Eichräume und Eichflächen von Unterschall- bzw. Überschall-5-Loch-Sonden, *Archiv für technisches Messen + messtechnische Praxis*, 42, 31–37, 1975. 9788

Boiffier, J.-L.: *The Dynamics of Flight – the Equations*, Wiley, Chichester, UK, 1998. 9786

5 Crawford, T. L. and Dobosy, R. J.: A sensitive fast-response probe to measure turbulence and heat flux from any airplane, *Boundary-Lay. Meteorol.*, 59, 257–278, 1992. 9784, 9785

Friehe, C. A., Burns, S. P., Khelif, D., and Song, X.: Meteorological and flux measurements from the NOAA WP3D aircraft in TOGA COARE, in: 8th Conference on Air-Sea Interaction, 28 January–2 February, Atlanta, GA, J42–J45, AMS, 1996. 9785

10 Haala, N., Cramer, M., Weimer, F., and Trittler, M.: Performance test on UAV-based photogrammetric data collection, in: UAV-g (unmanned aerial vehicle in geomatics) Conference, 14–16 September, Zurich, Switzerland, Vol. 16–20, American Meteorological Society, 2011. 9787

Haering, E. A.: *Airdata Calibration of a High-Performance Aircraft for Measuring Atmospheric Wind Profiles*, Tech. Mem. 101714, NASA, Edwards, CA, 24 pp., 1990. 9786

15 Khelif, D., Burns, S. P., and Friehe, C. A.: Improved wind measurements on research aircraft, *J. Atmos. Ocean. Tech.*, 16, 860–875, 1999. 9785

Kolmogorov, A.: The local structure of turbulence in incompressible viscous fluid for very large reynolds numbers, *Dokl. Akad. Nauk SSSR*, 30, 299–303, reprint: *Proc. R. Soc. Lond. A*, 1991, 434, 9–13, 1941. 9797

20 Leise, J. A. and Masters, J. M.: *Wind Measurements from Aircraft*, US Department of Commerce, National Oceanic and Atmospheric Administration, Aircraft Operation Center, Miami, Florida, USA, 1993. 9786

Lemonis, G., Schmücker, M., and Struck, H.: A fast response probe system for in-flight measurements of atmospheric turbulence, *Aerosp. Sci. Technol.*, 6, 233–243, 2002. 9784

25 Lenschow, D. H.: Aircraft measurements in the boundary layer, in: *Probing the Atmospheric Boundary Layer*, edited by: Lenschow, D. H., Am. Meteorol. Soc., Boston, MA, 39–53, 1986. 9786

Martin, S. and Bange, J.: The influence of aircraft speed variations on sensible heat flux measurements by different airborne systems, *Boundary-Lay. Meteorol.*, accepted for publication, 2013. 9785

30 Martin, S., Bange, J., and Beyrich, F.: Meteorological profiling of the lower troposphere using the research UAV “M²AV Carolo”, *Atmos. Meas. Tech.*, 4, 705–716, doi:10.5194/amt-4-705-2011, 2011. 9788

Multi-hole probes
with RPA

N. Wildmann et al.

Title Page

Abstract

Introduction

Conclusions

References

Tables

Figures

◀

▶

◀

▶

Back

Close

Full Screen / Esc

Printer-friendly Version

Interactive Discussion



- Pfau, A., Schlienger, J., Kalfas, A. I., and Abhari, R. S.: Virtual four Sensor Fast Response Aerodynamic Probe (FRAP), in: 16th Symposium on Measuring Techniques in Transonic and Supersonic Flow in Cascades and Turbomachines, 23–24 September, Cambridge, UK, 2002. 9784
- 5 Rosemount: Model 858 Flow Angle Sensors, Rosemount Inc., Bulletin 1014, Minneapolis, MN, 1982. 9785
- Sasangko, H.: Rand- und Spaltströmungen in stark gestaffelten Verdichtergittern aus schwach gewölbten Profilen, Technische Universität Braunschweig, ZLR-Forschungsbericht, 01, Braunschweig, Germany, 1997. 9788
- 10 Schlienger, J., Pfau, A., Kalfas, A. I., and Abhari, R. S.: Single pressure transducer probe for 3-D flow measurements, in: 16th Symposium on Measuring Techniques in Transonic and Supersonic Flow in Cascades and Turbomachines, 23–24 September, Cambridge, UK, 2002. 9784
- Semaan, R. and Scholz, P.: Pressure correction schemes and the use of the Wiener deconvolution method in pneumatic systems with short tubes, *Exp. Fluids*, 53, 829–837, 2012. 9790
- Smith, S. W.: *The Scientist and Engineer's Guide to Digital Signal Processing*, California Technical Publishing, San Diego, CA, USA, 1997. 9797
- Spieß, T.: *A Contribution to Turbulence Measurements with Autonomous Micro Aerial Vehicles*, Ph.D. thesis, Institute for Aerospace Systems, Techn. Univ. Braunschweig, Germany, 137 pp., 2006. 9788
- 20 Spieß, T., Bange, J., Buschmann, M., and Vörsmann, P.: First Application of the Meteorological Mini-UAV “M²AV”, *Meteorol. Z. N. F.*, 16, 159–169, 2007. 9785, 9788, 9790, 9807
- Sumner, D.: Calibration methods for a seven-hole pressure probe, in: *Sixth Triennial International Symposium on Fluid Control, Measurement and Visualization (Flucome 2000)*, edited by: Laneville, A., Sherbrooke, Canada, 6, 13–17 August, 2000. 9784
- 25 Telionis, D., Yang, Y., and Redinioti, O.: Recent developments in multi-hole probe (mhp) technology, in: *20th International Conference of Mechanical Engineering*, 15–20 November, Gramado, RS, Brazil, ABCM, 2009. 9784, 9785
- 30 Thomas, R. M., Lehmann, K., Nguyen, H., Jackson, D. L., Wolfe, D., and Ramanathan, V.: Measurement of turbulent water vapor fluxes using a lightweight unmanned aerial vehicle system, *Atmos. Meas. Tech.*, 5, 243–257, doi:10.5194/amt-5-243-2012, 2012. 9785

Multi-hole probes with RPA

N. Wildmann et al.

Title Page

Abstract

Introduction

Conclusions

References

Tables

Figures

◀

▶

◀

▶

Back

Close

Full Screen / Esc

Printer-friendly Version

Interactive Discussion



- Treaster, A. L. and Yocum, A. M.: The calibration and application of five-hole probes, *ISA Trans.*, 18, 23–34, 1979. 9788, 9789
- van den Kroonenberg, A. C., Martin, T., Buschmann, M., Bange, J., and Vörsmann, P.: Measuring the Wind Vector Using the Autonomous Mini Aerial Vehicle M²AV, *J. Atmos. Ocean. Tech.*, 25, 1969–1982, 2008. 9785, 9786, 9799
- 5 van den Kroonenberg, A., Martin, S., Beyrich, F., and Bange, J.: Spatially-averaged temperature structure parameter over a heterogeneous surface measured by an unmanned aerial vehicle, *Boundary-Lay. Meteorol.*, 142, 55–77, 2011. 9788
- Wildmann, N., Mauz, M., and Bange, J.: Two fast temperature sensors for probing of the atmospheric boundary layer using small remotely piloted aircraft (RPA), *Atmos. Meas. Tech.*, 6, 2101–2113, doi:10.5194/amt-6-2101-2013, 2013. 9787, 9796
- 10 Williams, A. and Marcotte, D.: Wind measurements on a maneuvering twin-engine turboprop aircraft accounting for flow distortion, *J. Atmos. Oceanic Technol.*, 17, 795–810, 2000. 9785, 9786
- 15 Zimmer, G., Alam, F., Watkins, S., and Peric, C.: Comparison of a high blockage wind tunnel, an open jet wind tunnel and on-road testing with respect to external surface pressures, in: *SAE Technical Paper 2001-01-1087*, SAE 2001 World Congress Detroit, 5–8 March, 2001. 9784

Table 1. Comparison of two methods to define dimensionless coefficients for five hole probe measurements.

	Bohn et al. (1975) (M ² AV)	Treaster and Yocum (1979) (MASC)
ΔP	$\left[\frac{1}{5} \sum_{i=0}^4 \left(P_i - \frac{1}{5} \sum_{j=0}^4 P_j \right)^2 \right]^{\frac{1}{2}}$ $+ \left[P_0 - \frac{1}{4} \sum_{i=1}^4 P_i \right]$	$\frac{(dP_1 + dP_2 + dP_3 + dP_4)}{4}$
k_α	$\frac{dP_01 - dP_03}{\Delta P}$	$\frac{dP_1 - dP_3}{dP_0 - \Delta P}$
k_β	$\frac{dP_02 - dP_04}{\Delta P}$	$\frac{dP_2 - dP_4}{dP_0 - \Delta P}$
k_q	$\frac{q - dP_{0s}}{\Delta P}$	$\frac{dP_0 - q}{dP_0 - \Delta P}$
k_p	$\frac{P_s + dP_{0s} - p}{\Delta P}$	$\frac{dP - p}{dP_0 - \Delta P}$

Title Page

Abstract Introduction

Conclusions References

Tables Figures

◀ ▶

◀ ▶

Back Close

Full Screen / Esc

Printer-friendly Version

Interactive Discussion





Fig. 1. Research RPA MASC.

AMTD

6, 9783–9818, 2013

Multi-hole probes with RPA

N. Wildmann et al.

Title Page

Abstract

Introduction

Conclusions

References

Tables

Figures

◀

▶

◀

▶

Back

Close

Full Screen / Esc

Printer-friendly Version

Interactive Discussion



**Multi-hole probes
with RPA**

N. Wildmann et al.

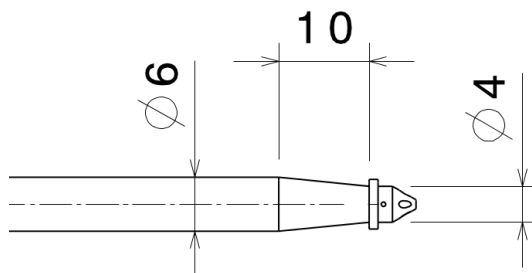
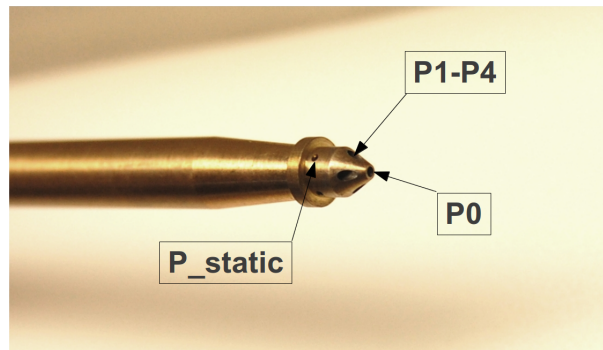


Fig. 2. Probe by ISM Braunschweig, picture and dimensions in mm.

[Title Page](#)[Abstract](#)[Introduction](#)[Conclusions](#)[References](#)[Tables](#)[Figures](#)[◀](#)[▶](#)[◀](#)[▶](#)[Back](#)[Close](#)[Full Screen / Esc](#)[Printer-friendly Version](#)[Interactive Discussion](#)

**Multi-hole probes
with RPA**

N. Wildmann et al.

Title Page

Abstract

Introduction

Conclusions

References

Tables

Figures

◀

▶

◀

▶

Back

Close

Full Screen / Esc

Printer-friendly Version

Interactive Discussion

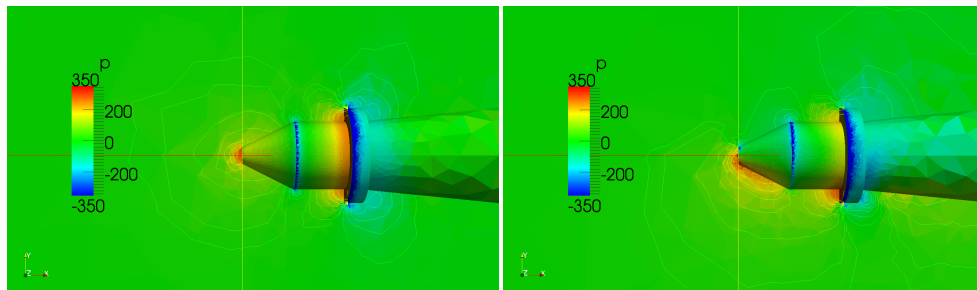


Fig. 3. OpenFOAM flow simulation around the probe tip at 24 ms^{-1} total airspeed at 0° angle of sideslip in both figures, 0° angle of attack in the left figure and 10° angle of attack in the right figure. The colour scale shows differential pressure to the environment in Pa.

Multi-hole probes with RPA

N. Wildmann et al.

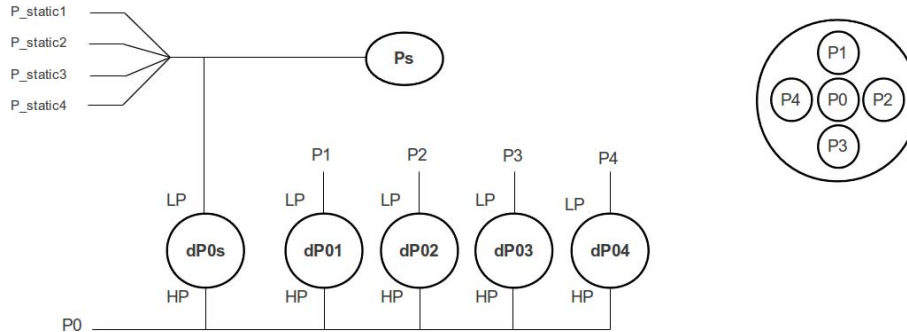


Fig. 4. Tubing system as used by the TU Braunschweig and described in Spieß et al. (2007) for the M²AV. The pressure transducer measurements $dP0i$ are differential pressure readings of the low pressure port (LP) connected to the holes P1–P4 and the ring port holes P_{static} compared to the high pressure port (HP), which in this case is the common port P0. Ps represents a barometric pressure sensor.

Title Page

Abstract

Introduction

Conclusions

References

Tables

Figures

◀

▶

◀

▶

Back

Close

Full Screen / Esc

Printer-friendly Version

Interactive Discussion



Multi-hole probes with RPA

N. Wildmann et al.

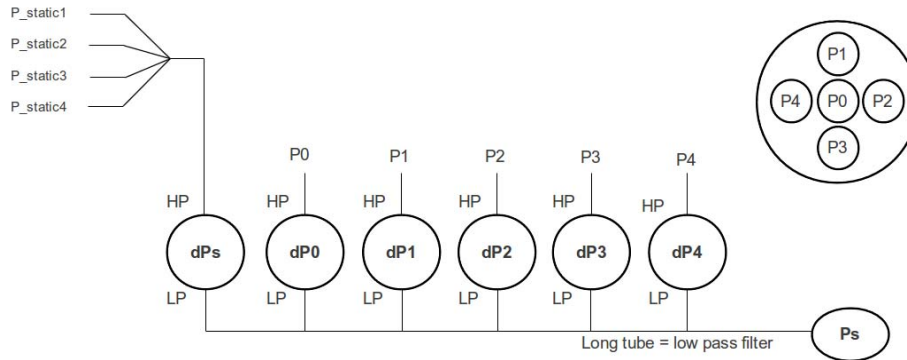


Fig. 5. Alternative tubing setup without branches as used in MASC. The pressure transducer measurements dP_i are readings of all single port pressures of the probe (P_0 – P_4 and P_{static}) compared to one common reference port. P_s represents a barometric pressure sensor.

Title Page

Abstract Introduction

Conclusions References

Tables Figures

◀ ▶

◀ ▶

Back Close

Full Screen / Esc

Printer-friendly Version

Interactive Discussion



**Multi-hole probes
with RPA**

N. Wildmann et al.

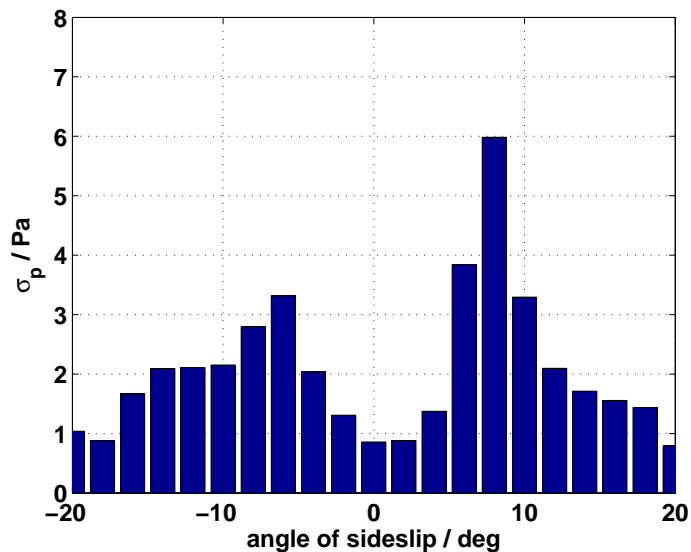


Fig. 6. Standard deviation of the pressure ports in front of the ring of the ISM probe during a windtunnel calibration. Angle of attack 10° , angle of sideslip shifted through -20 to 20° .

[Title Page](#)[Abstract](#)[Introduction](#)[Conclusions](#)[References](#)[Tables](#)[Figures](#)[◀](#)[▶](#)[◀](#)[▶](#)[Back](#)[Close](#)[Full Screen / Esc](#)[Printer-friendly Version](#)[Interactive Discussion](#)

Multi-hole probes
with RPA

N. Wildmann et al.

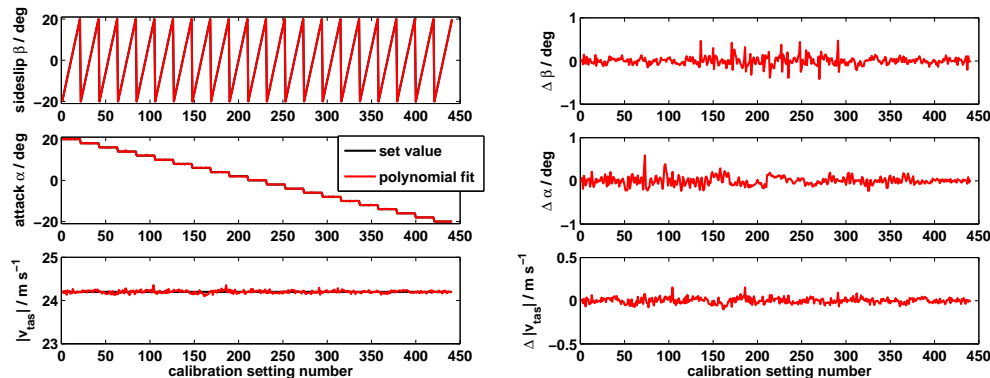


Fig. 7. Result of a windtunnel calibration of the MHP. The graph on the left shows mean values of 10 s at angle combinations between -20 and 20° for angle of attack and -20 to 20° sideslip. The black line is the angles and airspeed that were set in the windtunnel, the red line shows the result of the measurement after the polynomial fit. A polynomial fit of 9th order gives a maximum error of 0.47° and 0.59° for α and β respectively. The maximum error for true airspeed measurement is 0.15 m s^{-1} and can also include variations in the windtunnel speed. The graph on the right shows the corresponding errors for each calibration setting.

Multi-hole probes
with RPA

N. Wildmann et al.

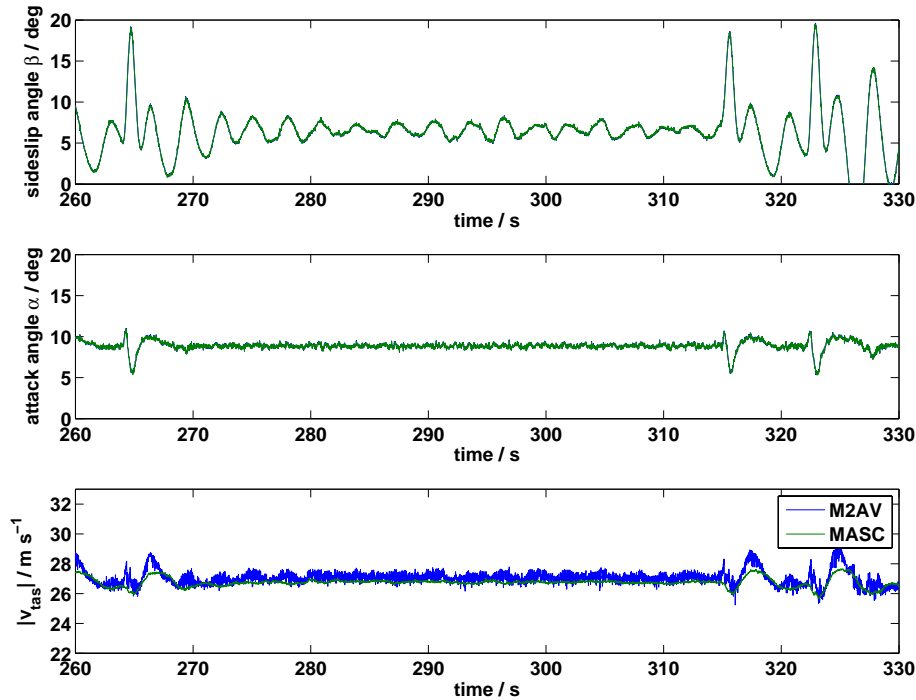


Fig. 8. True airspeed, measured with the five hole probe and calculated with the M²AV method, and the MASC method respectively. Angle of attack throughout the leg approx. 10°; angle of sideslip approx. 8°. Flight conditions, see text.

[Title Page](#)[Abstract](#)[Introduction](#)[Conclusions](#)[References](#)[Tables](#)[Figures](#)[◀](#)[▶](#)[◀](#)[▶](#)[Back](#)[Close](#)[Full Screen / Esc](#)[Printer-friendly Version](#)[Interactive Discussion](#)

Multi-hole probes
with RPA

N. Wildmann et al.

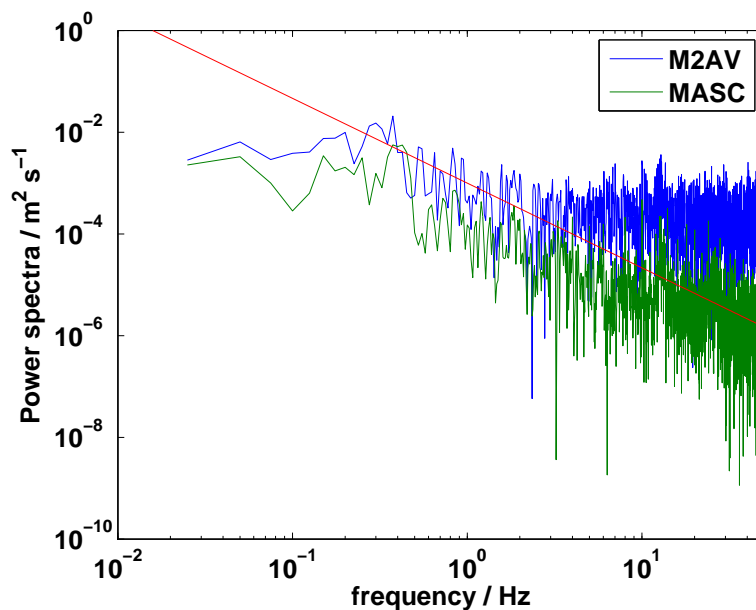


Fig. 9. Spectra of the true airspeed measurement in flight with standard calibration and new method. The red line shows the $k^{-3/5}$ slope.

[Title Page](#)[Abstract](#)[Introduction](#)[Conclusions](#)[References](#)[Tables](#)[Figures](#)[◀](#)[▶](#)[◀](#)[▶](#)[Back](#)[Close](#)[Full Screen / Esc](#)[Printer-friendly Version](#)[Interactive Discussion](#)

**Multi-hole probes
with RPA**

N. Wildmann et al.

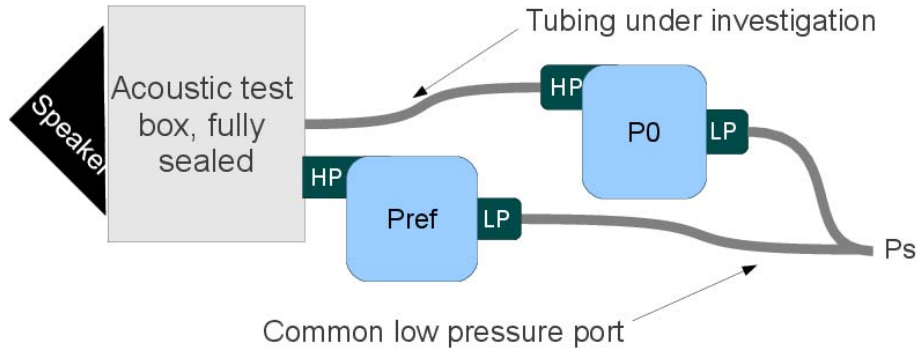


Fig. 10. Schematic drawing of the experiment to measure the tubing response. While the high pressure (HP) port of the reference transducer (Pref) is directly connected to the acoustic box, the HP port of the pressure measurement under investigation (P0) is connected with the necessary tubing of the real system. Ps is the common ambient pressure on the low pressure (LP) port of the transducers.

**Multi-hole probes
with RPA**

N. Wildmann et al.

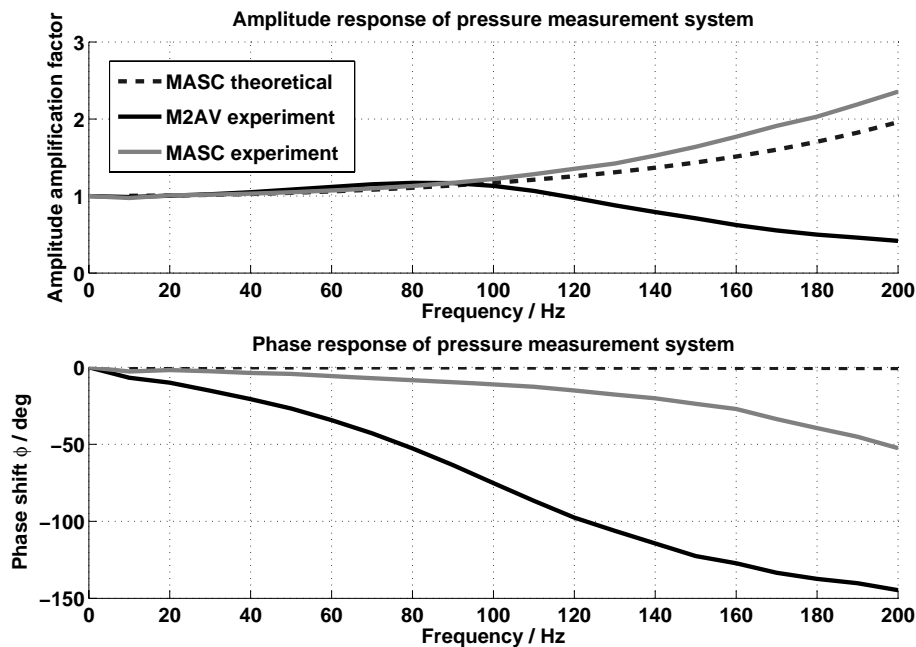


Fig. 11. Amplitude response of the pressure measurement system, including tubing, branches, transducer, etc.

Multi-hole probes
with RPA

N. Wildmann et al.

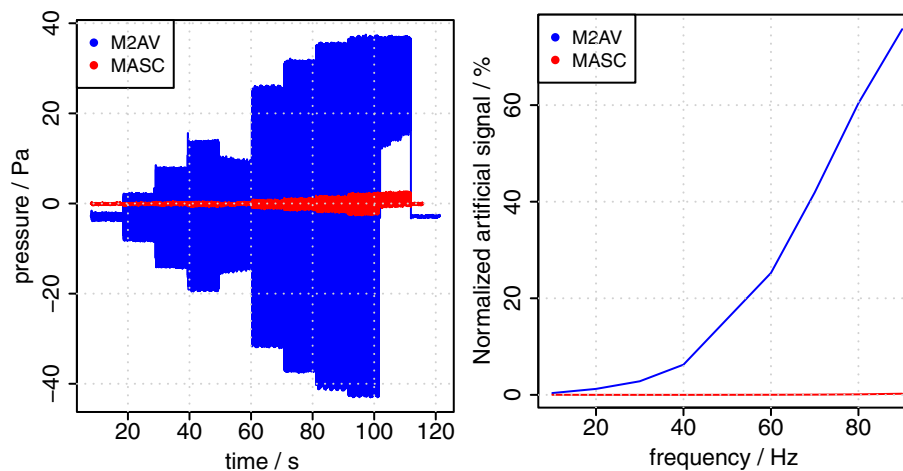


Fig. 12. Acoustic test of tubing system. Left: raw measurement of the transducers. Right: percentage of prevailing pressure that is measured as an artefact due to different phase shifts at high and low pressure port of the transducer.

Multi-hole probes with RPA

N. Wildmann et al.

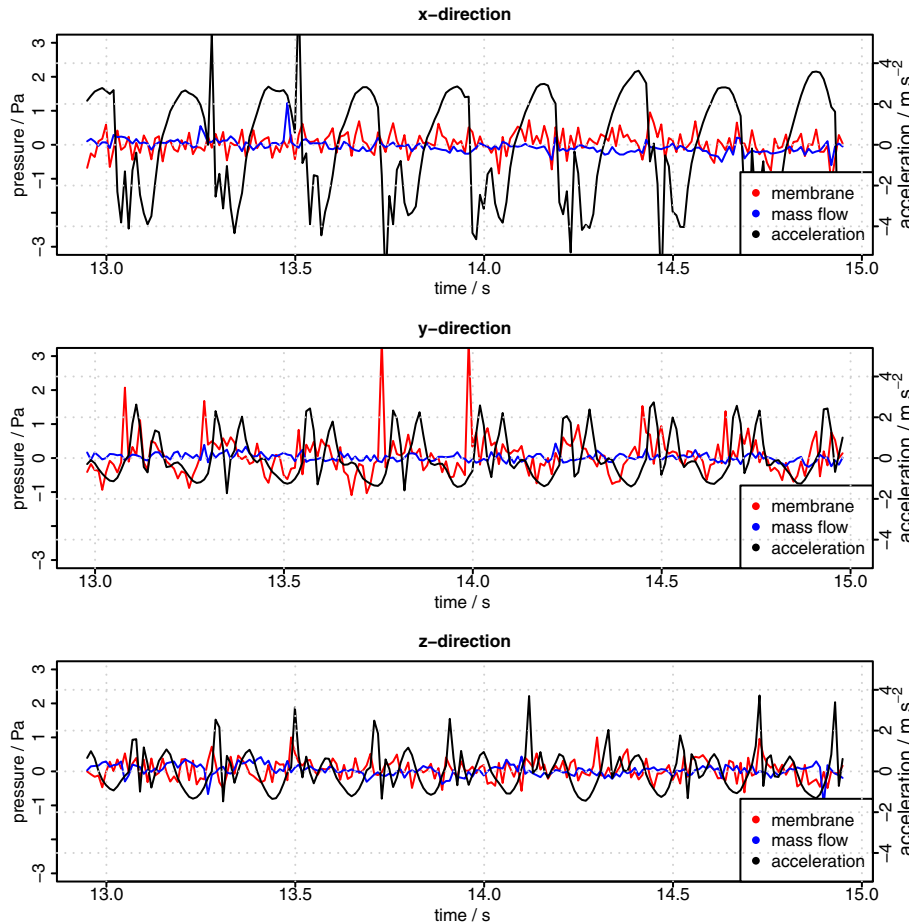


Fig. 13. Vibration/Acceleration applied to pressure transducers in distinct directions.

Title Page	
Abstract	Introduction
Conclusions	References
Tables	Figures
◀	▶
◀	▶
Back	Close
Full Screen / Esc	
Printer-friendly Version	
Interactive Discussion	



**Multi-hole probes
with RPA**

N. Wildmann et al.

Title Page

Abstract

Introduction

Conclusions

References

Tables

Figures

◀

▶

◀

▶

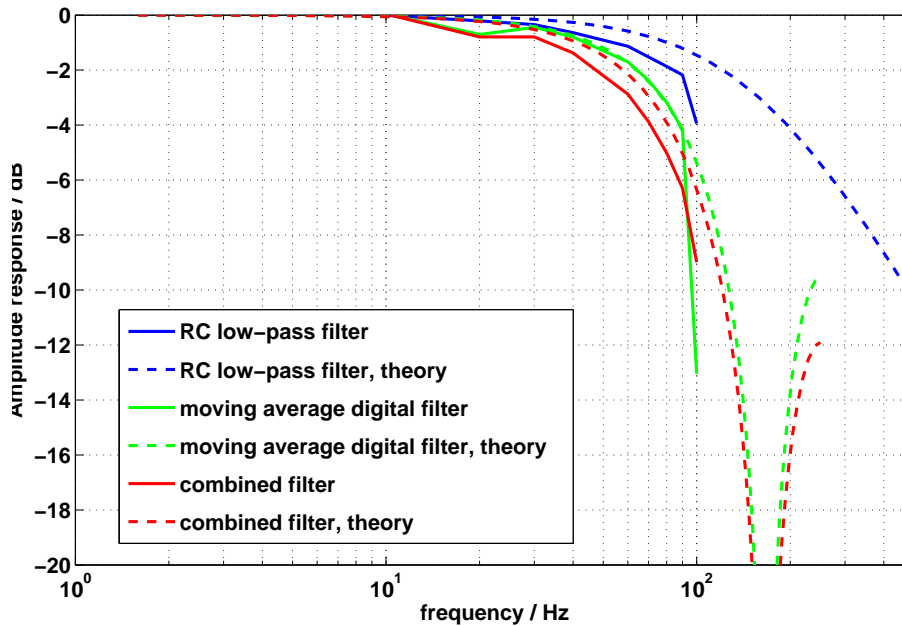
Back

Close

Full Screen / Esc

Printer-friendly Version

Interactive Discussion

**Fig. 14.** Amplitude response of filters in analog sensor channels.

Multi-hole probes
with RPA

N. Wildmann et al.

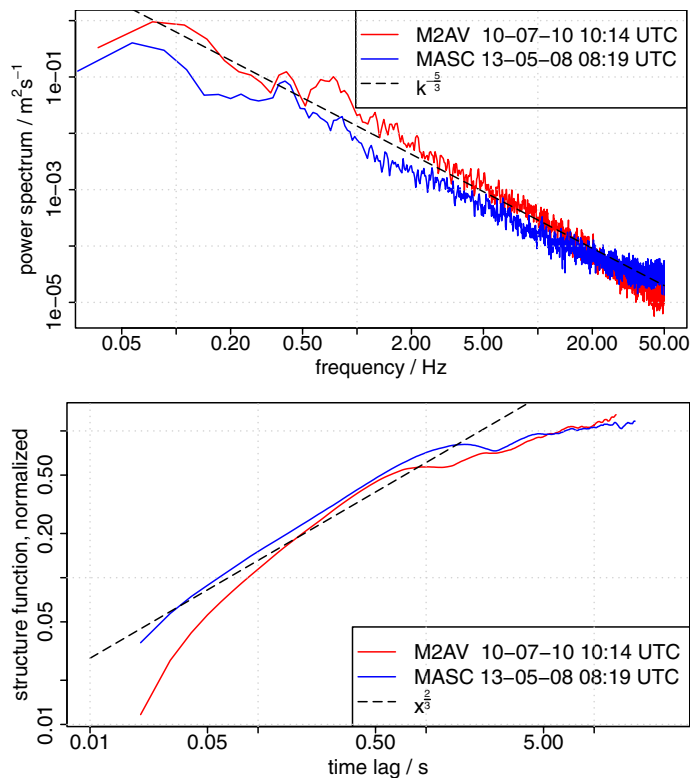


Fig. 15. A variance spectrum and a structure function of true airspeed measured with the MASC RPA in comparison to a measurement with the M²AV RPA. In both plots, the result is an average over 15 legs of 27 seconds each. The structure function is normalized by $2\sigma^2$ and therefore dimensionless. Flight conditions, see text.